Groundwater

Case Study/

# Imaging Hydrological Processes in Headwater Riparian Seeps with Time-Lapse Electrical Resistivity

by Mark R. Williams[1], Anthony R. Buda[2], Kamini Singha[3], Gordon J. Folmar[2], Herschel A. Elliott[4], and John P. Schmidt[5]

## Abstract

Delineating hydrologic and pedogenic factors influencing groundwater flow in riparian zones is central in understanding pathways of water and nutrient transport. In this study, we combined two-dimensional time-lapse electrical resistivity imaging (ERI) (depth of investigation approximately 2 m) with hydrometric monitoring to examine hydrological processes in the riparian area of FD-36, a small (0.4 $km^2$) agricultural headwater basin in the Valley and Ridge region of east-central Pennsylvania. We selected two contrasting study sites, including a seep with groundwater discharge and an adjacent area lacking such seepage. Both sites were underlain by a fragipan at 0.6 m. We then monitored changes in electrical resistivity, shallow groundwater, and nitrate-N concentrations as a series of storms transitioned the landscape from dry to wet conditions. Time-lapse ERI revealed different resistivity patterns between seep and non-seep areas during the study period. Notably, the seep displayed strong resistivity reductions (~60%) along a vertically aligned region of the soil profile, which coincided with strong upward hydraulic gradients recorded in a grid of nested piezometers (0.2- and 0.6-m depth). These patterns suggested a hydraulic connection between the seep and the nitrate-rich shallow groundwater system below the fragipan, which enabled groundwater and associated nitrate-N to discharge through the fragipan to the surface. In contrast, time-lapse ERI indicated no such connections in the non-seep area, with infiltrated rainwater presumably perched above the fragipan. Results highlight the value of pairing time-lapse ERI with hydrometric and water quality monitoring to illuminate possible groundwater and nutrient flow pathways to seeps in headwater riparian areas.

## Introduction

Hydrologic and chemical interactions in riparian zones profoundly influence the quantity and quality of water in small headwater streams, and therefore play an important role in shaping the integrity of downstream waters (Alexander et al. 2007). Riparian zones lie at the interface between terrestrial and aquatic environs (Gregory et al. 1991) where breaks in topographic slope or areas of heterogeneous soils and rock strata can promote groundwater discharge at distinct seepage faces (Winter et al. 1998), thereby inducing dynamic exchanges between local and regional groundwater systems (Winter 1988; Stein et al. 2004). In steeply sloped basins, characteristic of the Appalachian Mountains, these riparian seepage faces often form slope wetlands (Brinson 1993) or seeps. Seeps are of great import to the headwater

[1]Corresponding author: National Soil Erosion Research Lab, USDA-ARS, 275S. Russell St., West Lafayette, IN 47907; 765-494-8694; mark.williams2@ars.usda.gov

[2]Pasture Systems & Watershed Management Research Unit, USDA-ARS, 3702 Curtain Road, University Park, PA 16802.

[3]Department of Hydrologic Science and Engineering, Colorado School of Mines, Golden, CO 80401.

[4]Department of Agricultural & Biological Engineering, The Pennsylvania State University, 111 Hastings Road, University Park, PA 16802.

[5]Champaign Research Center, DuPont Pioneer, 985 County Road 300 East, Ivesdale, IL 61851.

*Article impact statement*: Time-lapse electrical resistivity imaging maps subsurface hydrological connections between riparian seeps and shallow groundwater.

Received January 2016, accepted August 2016.

doi: 10.1111/gwat.12461

hydrologic system as they collectively can supply between 50 and 80% of stream baseflow (Morley et al. 2011). In headwaters with groundwater nitrogen legacies, a problem common to parts of the Appalachian region (Gurdak and Qi 2012), riparian seeps with hydrologic connections to these nitrogen-rich aquifers can exert strong controls on stream water nitrate-N concentrations in forested (Burns et al. 1998; West et al. 2001; O'Driscoll and DeWalle 2010; Kaur et al. 2016) and agricultural (Williams et al. 2014, 2015) basins alike. Hence, delineating hydrologic and pedogenic factors influencing groundwater flow and discharge to riparian seeps is critical to their successful management and protection, as well as the headwater streams to which they drain.

Studies of the interactions between seeps and groundwater systems often are restricted to point-based hydrometric and chemical measurements. For instance, Vidon and Hill (2004a) employed a network of shallow wells and piezometers to monitor changes in groundwater levels over time in the glaciated region of southern Ontario, showing that discontinuities in peat layers promoted upward movement of groundwater that led to seep formation and nitrate-N efflux in the riparian zone (Vidon and Hill 2004b). Similarly, Angier and McCarty (2008) used piezometer transects in the mid-Atlantic coastal plain of Maryland to document groundwater upwelling and nitrate-N movement through shallow soil restrictive layers to riparian seeps. More recently, studies by Martínez-Santos et al. (2012) in Spain and Williams et al. (2014) in Pennsylvania applied insight from piezometry and groundwater chemistry to elucidate groundwater upwelling processes and associated nitrate-N transfers to seeps in stream riparian zones. While studies like these have shed new light on subsurface hydrological processes in riparian zones, they have been unable to sufficiently delineate subsurface heterogeneities leading to seep development and activation. Near-surface geophysics offers the opportunity to noninvasively survey the shallow subsurface, which can augment hydrologic insight from standard hydrometric monitoring to quantify the groundwater interactions in stream riparian zones (Parsekian et al. 2014).

Time-lapse electrical resistivity imaging (ERI) is an established near-surface geophysical technique that can be used to map dynamic subsurface hydrological processes in space and time (Singha et al. 2015). In essence, electrical conductivity (the reciprocal of electrical resistivity) measures the ability of soil and water to conduct electrical current (Keller and Frischknecht 1966). Because of its sensitivity to changes in electrical conductivity, time-lapse ERI has often been paired with saline tracer tests, thereby enabling hydrogeophysicists to track groundwater movement in riverine riparian zones (e.g., Doestch et al. 2012) and monitor hyporheic exchange processes in headwater streams (Ward et al. 2010). Time-lapse ERI also has been implemented without ionic tracers (i.e., under natural conditions) to understand interactions between surface water and groundwater in major river basins (Cardenas and Markowski 2011) and most recently, in large wetland complexes (Uhlemann et al. 2016). While the use of time-lapse ERI to unravel dynamic hydrological processes in stream and river corridors clearly is growing (Parsekian et al. 2014; Binley et al. 2015; Singha et al. 2015), its application to examining groundwater flow pathways to seeps remains underexplored to date (cf. Gentry and Burbey 2004), especially in riparian areas of small headwater agricultural watersheds.

In this case study, we applied time-lapse ERI over the course of several spring rainfall events to investigate the development and hydrologic activation of seeps in the riparian area of a headwater agricultural watershed where seeps collectively represent important sources of water and nutrients to the stream (Williams et al. 2014; 2015). We selected two distinct sites for monitoring in the riparian zone, including a seep area with evident groundwater discharge and an adjacent area lacking such seepage. Previous work at these sites using piezometry and two-component chemical mixing models (Williams et al. 2014) suggested riparian seeps received groundwater from a shallow fractured aquifer system that was confined below a fragipan soil horizon at about 0.6 m depth, while nearby areas without seeps lacked such vertical connectivity in the subsurface. Indeed, previous studies have documented anisotropic behavior in fragipans, where hydraulic conductivity, and hence preferential flow, can be greater in vertical rather than horizontal directions (Dabney and Selim 1987). Here, we look to corroborate vertical subsurface hydrological connections previously inferred from piezometers and explore the effects of soil heterogeneity on groundwater upwelling to riparian seeps with time-lapse ERI.

## Study Area

Our study took place in the FD-36 experimental watershed, a small (0.4 $km^2$) headwater agricultural basin located in the north central portion of the Mahantango Creek watershed (420 $km^2$) in east-central Pennsylvania (Figure 1a; Bryant et al. 2011). Watershed FD-36 is situated in the northeastern section of the nonglaciated, folded and faulted Appalachian Valley and Ridge Physiographic Province. Headwater streams (i.e., first-order perennial streams) in the Valley and Ridge region comprise between 50 and 100% of total stream length (Nadeau and Rains 2007), with Mahantango Creek representing the lower part of this range (~52% of streams are headwaters based on the National Hydrography Dataset). Like most headwater basins in the Valley and Ridge Province, FD-36 is underlain by highly fractured and weathered bedrock at shallow depths (Wyrick and Borchers 1981). This fractured zone, which extends to 15 m below the surface in places, supports an aquifer system that gives rise to numerous springs and seeps in the riparian area (Gburek and Urban 1990) and also serves as the primary water source to headwater streams, supplying upward of 80% of annual streamflow (Gburek et al. 1999). In agricultural watersheds like FD-36, recharge of the shallow fractured aquifer often occurs in cropped fields where manures and fertilizers are applied, thereby leading to N leaching and a concomitant buildup of nitrate-N in groundwater (Pionke

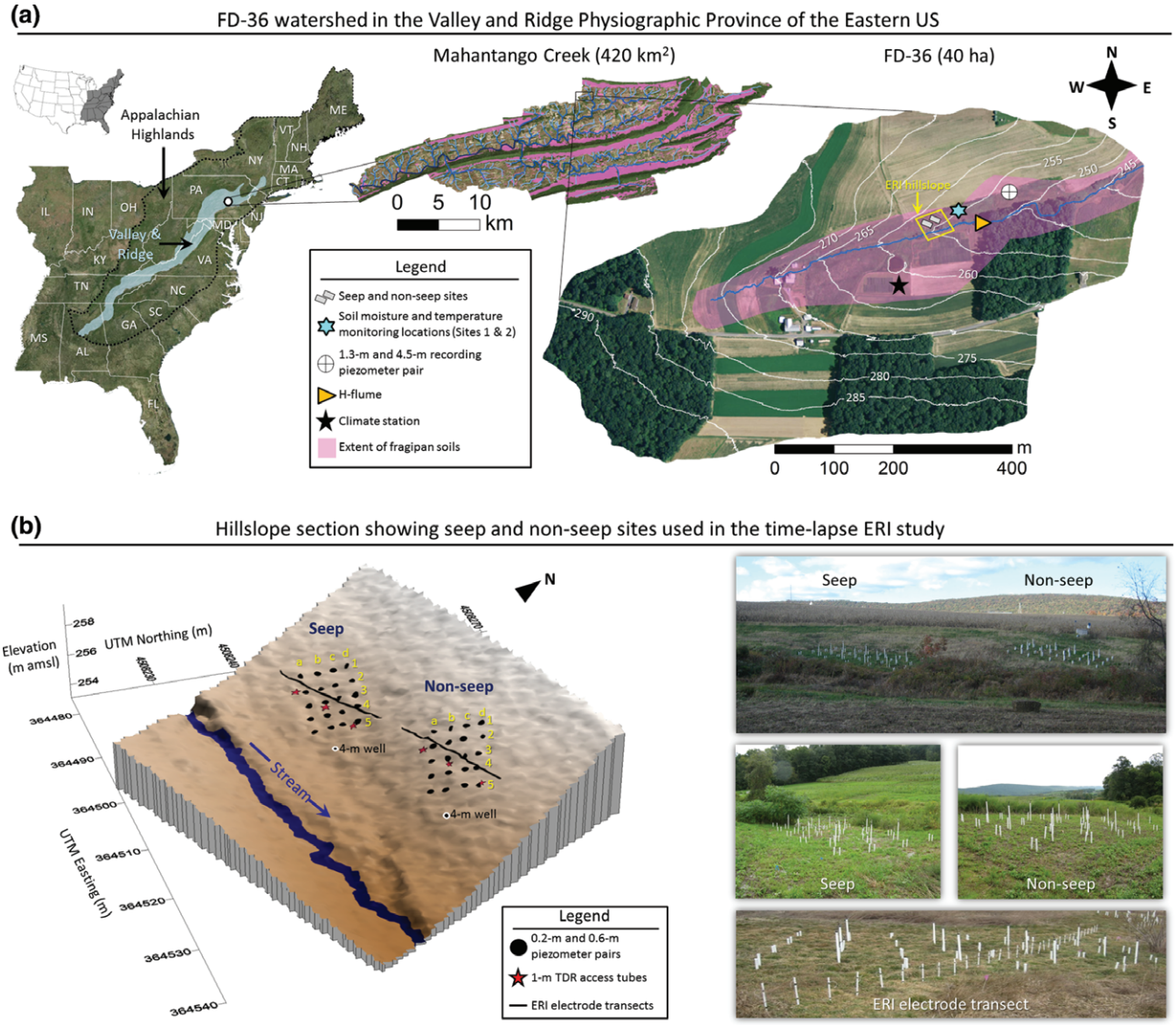


**Figure 1. Site map showing (a) the location of the FD-36 watershed in the Mahantango Creek experimental basin and in the Valley and Ridge region of the Eastern US and (b) the experimental hillslope in FD-36 where seep and non-seep sites were instrumented with piezometers and assessed with time-lapse ERI.**

and Urban 1985) that affects the water quality of riparian seeps (Williams et al. 2015) and streams (Gburek and Folmar 1999).

Watershed FD-36 is a moderately sloped basin with soils largely derived from red shale, mudstone, and sandstone parent materials. Elevations range from 242 to 294 m amsl (Figure 1a), with ridgetop and valley locations possessing slopes between 1 and 10% and hillslopes as steep as 25%. The majority of the watershed is underlain by the Irish Valley Member of the Catskill Formation, which includes alternating beds of olive-gray sandstone, siltstone, red shale, and mudstone (Geyer and Wilshusen 1982). Soil catenas are characteristic of those found in the Valley and Ridge Province of Pennsylvania (Ciolkosz et al. 1979; Ciolkosz et al. 1990), with well-drained residual soils that are usually stony, silt loams (Leck Kill, Calvin, and Berks series) occupying the ridge tops and side slopes, and colluvial soils with fragipan horizons (Albrights and Hustontown series) found mainly along the stream corridor (Williams et al. 2014; Figure 1a). Notably, fragipans in FD-36 tend to begin at depths ranging from 0.4 to 0.8 m (Gburek et al. 2006), and these horizons often act as confining layers, separating shallow perched water tables from the nitrogen-rich fractured aquifer system below (Hill 1990; Williams et al. 2014).

Climatic and land-use conditions in FD-36 typify those found in agricultural areas of east-central Pennsylvania. The climate is temperate and humid, with annual precipitation around 1080 mm/year (Buda et al. 2011) and mean annual temperatures ranging from 10 to 11 °C (Lu et al. 2015). Land-use is predominately agriculture (56%), with woodlots (30%) and grassland (13%) occupying the rest of the basin (Figure 1a). Side slopes and shoulders feature cropped fields with well-drained soils that are typically planted in 3- to 4-year rotations of corn, small grains, hay, and soybeans. These fields routinely receive manure

**Table 1**
**General Properties of the Hustontown Soil Underlying the Seep and Non-Seep Sites (from Lindeburg 2011)**

| Horizon | Depth (cm) | Texture | Sand % | Silt % | Clay % | Bulk Density ($g/cm^3$) | Porosity (%) |
|---|---|---|---|---|---|---|---|
| Ap1 | 0 to 18 | Silt | 25.7 | 56.9 | 17.4 | 1.2 | 54 |
| Ap2 | 18 to 30 | Silt | 28.8 | 54.7 | 16.6 | 1.6 | 41 |
| Bt | 30 to 56 | Loam | 31.0 | 48.8 | 20.2 | 1.6 | 38 |
| Bx1 | 56 to 89 | Loam | 41.9 | 40.1 | 18.1 | 1.7 | 37 |
| Bx2 | 89 to 124 | Clay | 29.8 | 39.2 | 31.0 | 1.7 | 36 |

Note: Soil texture, particle size distribution, bulk density, and porosity were analyzed with standard USDA methods (Soil Survey Staff 2014).

and fertilizer in spring and fall, with fall being a particularly sensitive period for N leaching (Heathwaite et al. 2000) that can ultimately lead to elevated nitrate-N levels in shallow groundwater (Pionke and Urban 1985) and in riparian seeps (Williams et al. 2015). Footslopes and toe slopes, including the riparian area, have poorly drained soils that preclude agricultural management, and are typically planted with warm and cool season grasses.

## Selection of Time-Lapse ERI Site

We selected a riparian area on a south-facing hillslope in FD-36 for the time-lapse ERI study (Figure 1a and b). Soils were classified as a moderately well-drained Hustontown silt loam (see Table 1 for general soil properties), which possessed a reasonably well-developed fragipan beginning at a depth of about 0.6 m. Previous research by Williams et al. (2014) informed our choice of neighboring seep and non-seep areas for time-lapse ERI monitoring. Both locations were moderately sloped, with average gradients ranging from 16% in the seep area to 18% in the non-seep area. Planform curvature in the seep area was laterally concave with convergent topography, while the non-seep area was laterally convex, indicating a tendency for flow divergence. Field reconnaissance showed that the seep exhibited intermittent to occasionally perennial flow (dependent on seasonal rainfall amounts), and responded quickly to precipitation events. Moreover, evidence from point-based hydrometric monitoring, chemical mixing models, and spatial analyses of field management data suggested that these two sites displayed interesting contrasts in surface water and groundwater interactions, with the seep potentially connected to a shallow fractured aquifer with high nitrate-N levels from upslope recharge zones in agricultural fields, and the non-seep area lacking any apparent linkage between perched and regional groundwater (Williams et al. 2014; 2015).

## Materials and Methods

### Hydrometric and Water Quality Monitoring

We collected information on shallow groundwater and soil moisture in seep and non-seep areas to provide supportive hydrologic data for the time-lapse ERI surveys. Shallow groundwater monitoring in seep and non-seep areas was accomplished with five transects of nested piezometers arrayed in a grid with dimensions of 8.8 m by 5.1 m (Williams et al. 2014). Each transect within the grid contained four pairs of piezometers spaced 1.5 m apart. Each piezometer pair consisted of a shallow (0.2 m) and deep (0.6 m) piezometer, which appropriately captured major soil features at each site (0.2 m – Ap horizon border; 0.6 m – top of fragipan). A 4-m deep piezometer located immediately downslope of the seep and non-seep sites permitted groundwater monitoring when water tables were below 0.6 m. All piezometers were constructed using 5-cm diameter PVC pipe, with shallow piezometers screened at the bottom 0.08 m and 4-m piezometers screened at the bottom 0.5 m (Figure 2). Installation of piezometers featured a sand pack added to the height of the screen, followed by a bentonite plug to fill the annular space from the top of the screen to the ground surface.

All hydrometric and water quality measurements were performed on the same days as ERI monitoring. Hydraulic head was determined by measuring depth-to-groundwater in each piezometer with a high-precision water level indicator (Durham Geo Slope-Enterprises, Inc., Mukilteo, Washington) and then referencing the measurements to a common elevation datum. In addition to groundwater monitoring, we tracked changes in soil moisture using time-domain reflectometry (TDR). Briefly, three TDR access tubes (1-m deep) were installed across each transect (Figures 1b and 2). On each of the hydrometric monitoring dates, a Trime-FM TDR probe (IMKO, Ettlingen, Germany) was inserted into the access tubes and soil water content was measured at 0.2 m depth intervals (0.2, 0.4, 0.6, 0.8 m) over the length of the tube. Finally, nitrate-N concentrations in shallow groundwater were assessed at both sites. Shallow piezometers (0.2 and 0.6 m) were purged with a peristaltic pump after water level measurements and ERI surveys had been done, and water samples were then collected in 125 mL plastic (HDPE) bottles and stored at 4 °C until analysis. Water samples were filtered (0.45 µm) in the lab and then analyzed with a Lachat QuickChem FIA+ autoanalyzer (QuickChem Methods FIA+ 800 Series, Lachat Instruments, Loveland, Colorado) for nitrate-N.

In order to place site-specific hydrometric and resistivity data in context, we also leveraged continuous (5-min interval) meteorological and hydrological datasets from parallel research initiatives in the FD-36 watershed

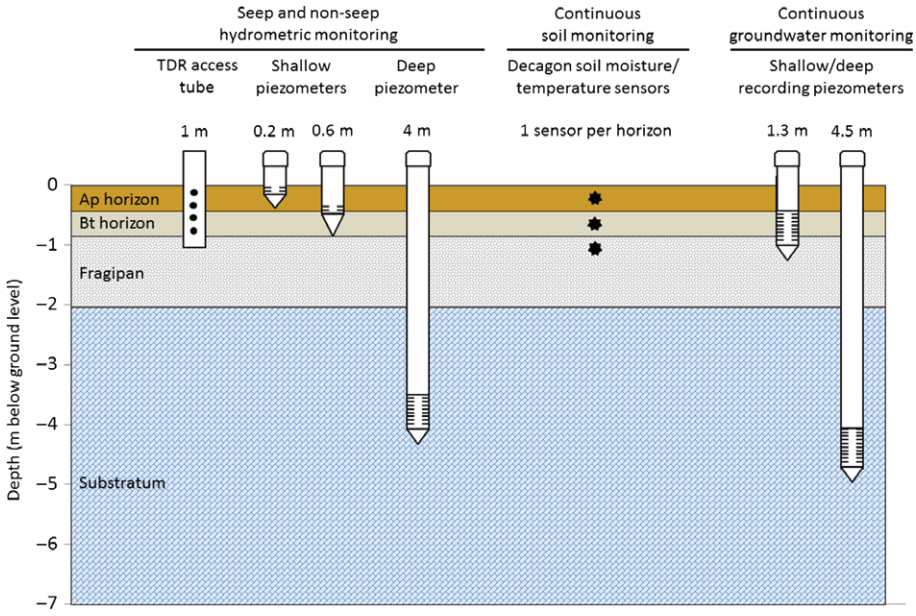


**Figure 2. Generalized cross section of the soils underlying the south hillslope of FD-36 showing the installation depths and design of hydrometric monitoring equipment at seep and non-seep ERI locations, as well as the layouts for continuous soil and groundwater monitoring at nearby locations along the south hillslope in FD-36 (see Figure 1a).**

(Figure 1b). All datasets covered the 7-week time frame from April 4 to May 23, 2012, which generally encompassed the period during which ERI surveys were conducted. Air temperature and rainfall data were obtained from a Campbell Scientific meteorological station (Campbell Scientific, Inc., Logan, Utah) in the middle of the watershed (Figure 1a). In addition, two hillslope trenches (Sites 1 and 2; Figure 1a) adjacent to the seep and non-seep locations (about 35 m away) provided soil moisture and temperature data, which were monitored with Decagon 5TE sensors (Decagon Devices, Pullman, Washington) installed in the middle of the Ap, B, and Bx (fragipan) horizons (sensor depths ~ 0.15, 0.5, and 1 m) at each site (Figure 2). Soil moisture and temperature data from each site were averaged across all three horizons to provide insight into temporal changes in soil conditions in the upper 1 m of soil. A pair of shallow (1.3 m) and deep (4.5 m) recording piezometers located on the same hillslope as the seep and non-seep sites (about 150 m downstream) provided data on groundwater dynamics (Figure 1a). Both piezometers were screened at the bottom 0.5 m (Figure 2), with the shallow piezometer installed above the fragipan and the deep piezometer penetrating the upper part of the fractured aquifer. Water levels in both piezometers were monitored with Odyssey capacitance sensors (Dataflow Systems, Inc., Christchurch, New Zealand). Finally, continuous streamflow data were acquired from a recording H-flume about 75 m downstream of the ERI survey sites.

### Time-Lapse ERI Surveys

We used time-lapse ERI monitoring to image subsurface hydrological processes in seep and non-seep areas over a 1-month period (April 21 to May 21, 2012) in which a series of storm events transitioned riparian soils from a dry to a wet state. The value in using the time-lapse ERI approach is that it captures seep and non-seep sites in a defined background state and describes their evolution as the riparian landscape wets up. In essence, changes in geophysical response relative to the background state at both sites can be linked to hydrological change, assuming that changes in electrical resistivity are primarily related to variations in water content and that other variables including temperature, salinity, and the composition and arrangement of soil particles, vary minimally during the time-lapse surveys or can properly be accounted for post hoc (Samouëlian et al. 2005). While continuous hydrometric data provided critical insight into changes in soil moisture and temperature during the ERI surveys, we did not collect site-specific data on the electrical conductivity of groundwater. Nevertheless, monthly groundwater monitoring in the shallow fractured aquifer showed the electrical conductivity of surficial groundwater averaged 195 $\mu$S/cm from 2011 to 2012, with a coefficient of variation less than 3% indicating temporal changes in groundwater chemistry were generally small.

In early April 2012, we established ERI sampling transects bisecting a seep and an adjacent non-seep area in the riparian zone. Each transect ran roughly parallel to the stream (Figure 1b) and featured 32 stainless steel electrodes spaced 0.5 m apart, yielding a total transect length of 15.5 m. We chose a dipole-dipole array because of its inherent strength in resolving lateral changes in resistivity (Samouëlian et al. 2005; Loke 2015). Dipoles were collected from skip-0 to skip-9, yielding 259 quadripoles in total for each data set over a period of approximately 30 min. We were most interested in the upper 2 m of soil, which included the critical region above and below

the fragipan horizon at each site. Although surface soils were relatively dry ($\theta_{seep} = 18.7\%$; $\theta_{non\text{-}seep} = 15.7\%$) during the installation, contact resistances between the electrodes and the ground were less than 10 kohm, which we considered good. Electrodes remained in the ground for the duration of the study to guarantee consistency between surveys, and contact resistance checks were performed prior to each survey. Also, close cooperation with local landowners assured that the electrode transects and associated monitoring equipment were not disturbed by agricultural activities at any point during the study.

Five ERI surveys were performed in seep and non-seep areas using an IRIS Syscal Pro Resistivity Meter (IRIS Instruments, Orleans, France), with the first survey on April 21, 2012 providing background resistivity data, and subsequent surveys characterizing hydrological changes in seeps and non-seeps after rainfall events. Repeat measurements, or stacks, were used to help quantify measurement error. Up to three stacks were collected during surveys, with a mean stacking error of 0.2%. Two-dimensional distributions of soil resistivity in seep and non-seep areas were obtained by inverting the field resistance data with EarthImager2D (Advanced Geosciences, Inc.). To assess resistivity changes over time, we used a difference inversion approach, which looks at ratios of the resistances collected in the field. This approach has been widely used to estimate changes in resistivity relative to background conditions in hydrological studies with time-lapse ERI (Daily et al. 1992; Cassiani et al. 2009). We applied the temperature-correction method of Hayley et al. (2007) to calculate resistivity values at a reference temperature of 25 °C, which allowed us to account for variable soil temperatures experienced during 2-month time-lapse ERI study. Additional details on parameters used in data collection and the inversions are given in Table 2.

**Table 2**
**Time-Lapse ERI Parameters Used in Seep and Non-Seep Surveys**

| ERI parameters | Seep and non-seep study areas |
|---|---|
| Electrode array | Dipole-dipole |
| Number of electrodes | 32 |
| Number data points | 259 |
| Electrode spacing ($a$) | 0.5 m |
| Separation factor ($n$) | 0 to 9 |
| Length of transect | 15.5 m |
| Depth of investigation | 1.6 m |
| Number of stacks | 2 to 3 |
| Stacking error | 0.2% |
| Current injection time window | 1 s |
| Resistance check | Prior to all surveys |
| Number of channels | Up to 10 channels used |
| Duration of the survey | 28 min |
| Static inversion parameters | Final absolute error approximately 2.5% |
| Time-lapse inversion parameters | Simultaneous inversion (data difference)<br>First background image as reference |

## Results and Discussion

### General Patterns in Climate, Hydrology, and Soil Conditions

The 90-day period prior to the background ERI surveys on April 21, 2012 was quite dry. Precipitation totaled 76 mm from January 20 to April 20, 2012, which was 45% of the 5-year (2007 to 2011) mean precipitation amount over the same time frame. Notably, only 3 mm of rain fell over the eighteen days prior to April 20, 2012 (Figure 3a). Mean daily air temperatures were 11.3 °C, with daily mean temperatures ranging from 4.7 to 22.1 °C (Figure 3b). Volumetric moisture content on the south hillslope reflected the effects of the 3-month dry spell, generally averaging 22 to 29% in the top 1 m of soil, which was slightly less than the estimated field capacity of 31% for Hustontown soils (determined using empirical relationships with soil texture and organic matter; Saxton and Rawls 2006). In addition, soil temperatures mostly held steady at 10 °C from April 4 to April 14, 2012 before increasing to 13 to 15 °C in response to a 6-day warm interval that began on April 15, 2012. Water tables were well below 0.6 m at seep and non-seep sites, as well as in the continuously monitored shallow recording piezometer (Figure 3e), indicating the near absence of a perched water table along most of the south hillslope in FD-36 due to dry conditions. Likewise, water levels in the deep recording piezometer also responded to limited rainfall by declining 0.3 m between April 4 and April 21, 2012. Streamflow remained at or below 0.5 L/s for the duration of the period (Figure 3f).

The 6-week period following the background ERI surveys on April 21, 2012 (collected from 1100 to 1200 EDT) was punctuated by three distinct storm events, as well as occasionally lighter rainfalls that brought rainfall totals to 141 mm by the end of the study (Figure 3a). The first storm began on April 21, 2012 (~1430 EDT) and lasted 2 days, delivering 40.1 mm of rainfall. Subsequent storms on May 7 to 8, 2012 and May 14 to 15, 2012 added 30.7 and 42.9 mm of rainfall, respectively. Each rainfall event resulted in significant and rapid water table rises in the shallow recording piezometer, indicating the development of perched water tables above the fragipan that responded immediately to rainfall inputs (Figure 3e). Water levels in the deep recording piezometer always were above those recorded in the shallow piezometer (indicating a potential upward flow gradient), and its response to rainfall was generally muted and somewhat lagged relative to the shallow piezometer (Figure 3e). This pattern continued through the last rainfall event when water levels in the deeper piezometer ultimately rose above the land surface, indicating artesian conditions in the fractured aquifer. Artesian conditions were likely

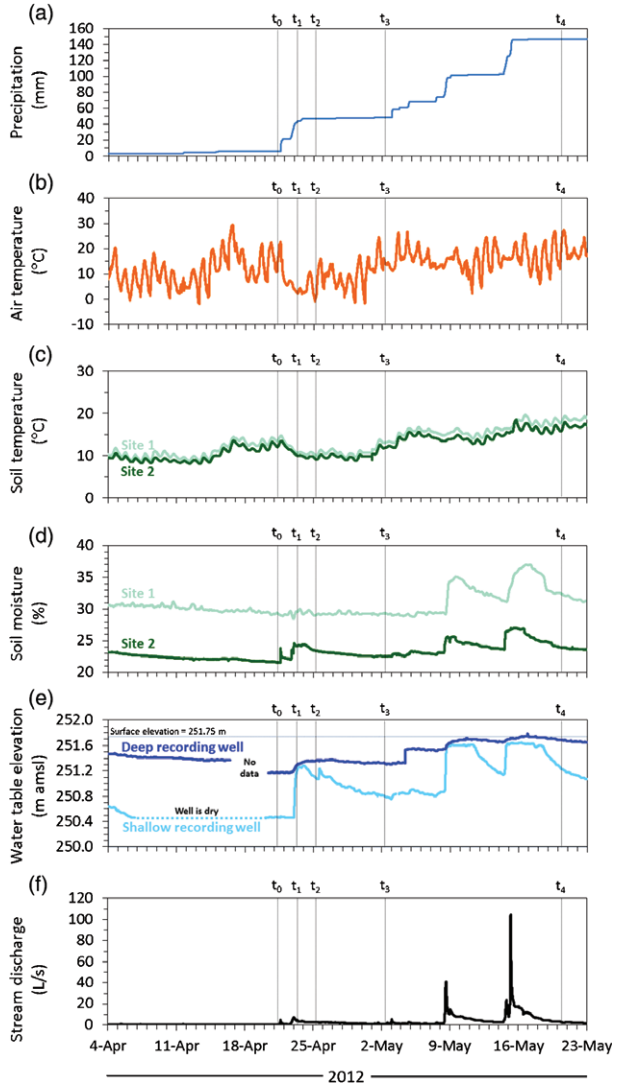


**Figure 3. Temporal changes in climate, soil, and hydrologic conditions from April 4 to May 23, 2012, including (a) cumulative precipitation (mm), (b) air temperature (°C), (c) soil temperature (°C)*, (d) soil moisture (%)*, (e) water table elevations (m amsl), and (f) stream discharge (L/s). Vertical dashed lines indicate the timing of the background ERI survey ($t_0$ = April 21, 2012) as well as the four subsequent surveys conducted over the 1-month wet-up period ($t_1$ = April 23, 2012; $t_2$ = April 25, 2012; $t_3$ = May 2, 2012; $t_4$ = May 21, 2012). *Continuous soil moisture and temperature measurements were made with Decagon 5TE sensors.**

induced by the presence of the fragipan, which was acting as an aquitard in the riparian area along the south-facing hillslope in FD-36. Streamflow and soil moisture rose subtly after the first storm, reflecting the effects of dry antecedent conditions, but then increased markedly after the second and third storm events, with moisture levels rising briefly above field capacity (Figure 3d) and peak stream discharge increasing 25- and 66-fold over pre-storm baseflows of 1.6 L/s (Figure 3f). Soil temperatures generally mirrored air temperatures (Figure 3b, c), with soils gradually warming from 13 °C prior to the background survey to 17 °C on May 21, 2012 (Figure 3c).

### Background Resistivity of Seep and Non-Seep Areas

Two-dimensional background resistivity models provided important insight into subsurface characteristics of riparian soils in the seep and non-seep sampling areas ($t_0$ in Figures 4 and 5). In general, resistivity in seep and non-seep areas ranged from 150 to 650 Ωm, within the typical range for largely saturated soils and alluvial sediments (Loke 2015). Notably, background resistivity tomograms in the seep area were much more diverse than those in the non-seep area. Because resistivity inversions were corrected for temperature deviations during the study period, and other major factors such as soil properties (e.g., texture, porosity) were assumed similar between the two sites (see Table 1), we hypothesized that variable saturation induced by the seep zone was the driving factor explaining the greater heterogeneity in resistivity in the seep area relative to the non-seep area. We explore this possibility in greater detail below.

In the non-seep area ($t_0$ in Figure 4), a distinct horizontal layer of high resistivity (400 to 650 Ωm) was apparent below about 0.6 m depth in the background inversion, with a much lower resistivity region (150 to 300 Ωm) situated above it. The low resistivity region roughly corresponded with the location of the Ap horizon, which is mapped from 0 to 0.3 m, with the higher resistivity region below it suggesting a relatively homogenous fragipan horizon that begins around 0.6 m. Increased resistivity in the fragipan horizon may be due in part to changes in soil bulk density, which increases from about 1.4 g/cm$^3$ in the Ap horizon to 1.7 g/cm$^3$ in the fragipan (Table 1). In an electrical resistivity study of fragipan soils in the Palouse Region of northern Idaho, Leslie and Heinse (2013) observed that the most dense soil horizons also were the most resistive, although these effects likely were amplified by low soil water contents at their site. Certainly, well-developed fragipans in the eastern US typically possess low soil water contents due to their high bulk density and low hydraulic conductivity (Grossman and Carlisle 1969). In the non-seep area, which appeared to possess a consistent fragipan horizon, soil moisture was only 23.7% at 0.8 m depth (just below the top of the fragipan) ($t_0$ in Figure 4). In contrast, soil moisture at the same depth in the seep area was substantially greater at 43.0% ($t_0$ in Figure 5), suggesting a possible influence of groundwater discharge at that location.

As discussed above, relationships between resistivity patterns and soil characteristics in the seep region suggested much greater heterogeneity in the subsurface ($t_0$ in Figure 5) relative to the adjacent non-seep area. In general, pockets of high resistivity (400 to 650 Ωm) were found in the upper 1 m of the inversion while lower resistivity values (150 to 250 Ωm) largely were confined to depths greater than 1 m. Several vertically aligned areas of low resistivity were noted in the seep area, with the one occurring between 7 and 8 m on the ERI transect being the most prominent. These vertically oriented low-resistivity anomalies may indicate zones of elevated moisture resulting from preferential water

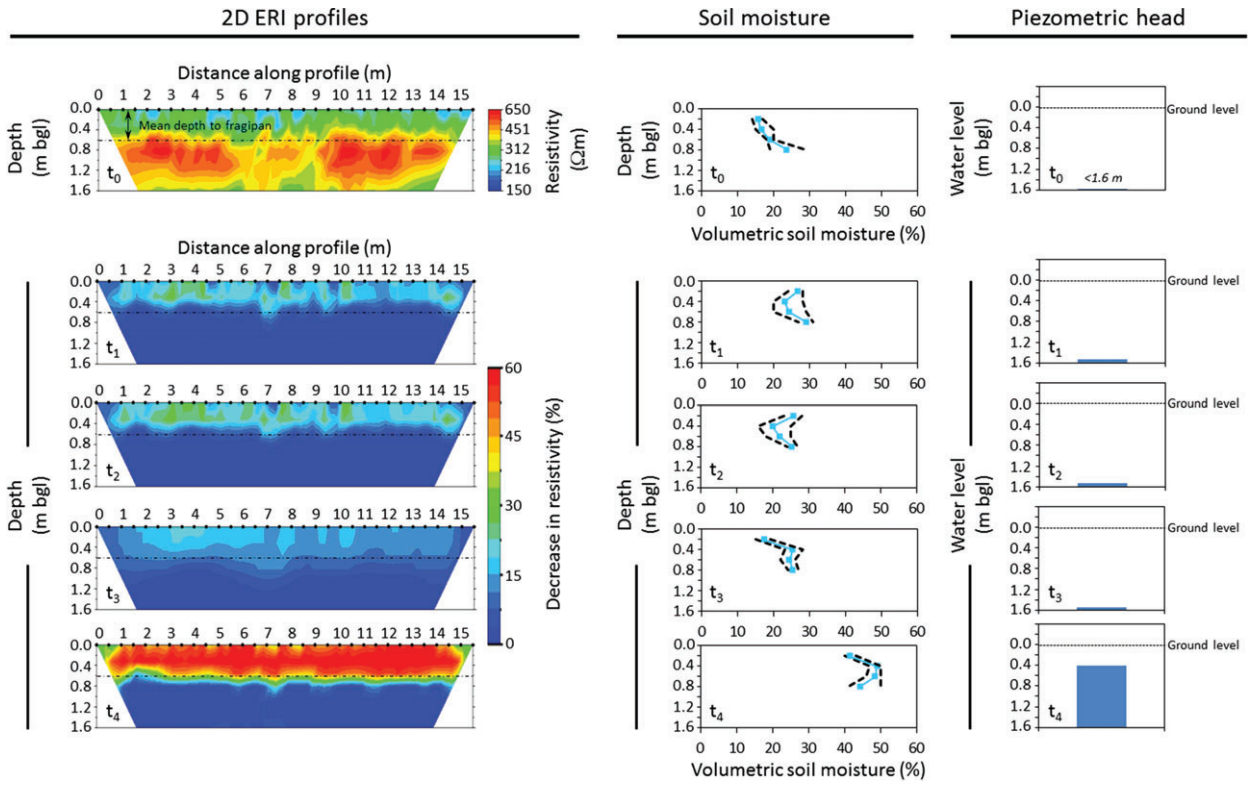


**Figure 4. Non-seep resistivity tomograms, soil moisture patterns, and piezometric head (4-m piezometer) for background conditions ($t_0$ = April 21, 2012) and four subsequent time steps over the 1-month wet-up period ($t_1$ = April 23, 2012; $t_2$ = April 25, 2012; $t_3$ = May 2, 2012; $t_4$ = May 21, 2012). Background resistivity data are given in Ωm, whereas resistivity difference inversions are shown as the percentage difference from background conditions. Volumetric soil moisture* is plotted as a function of depth, with minimum and maximum values shown as dashed black lines and the means shown as a solid blue line. Piezometric head is shown as water level depth (m) below ground level (bgl). *Volumetric soil moisture was measured with a Trime-FM TDR probe at three locations along the electrode transect, and mean, minimum, and maximum values were calculated across all three locations for each of the four depth intervals.**

movement through discontinuities in the fragipan in the vicinity of the seep. Indeed, volumetric water content measurements taken with TDR along the ERI transect showed a marked transition from dry conditions at the surface (18.7%) to fully saturated conditions at 0.8 m (43.0%) ($t_0$ in Figure 5), suggesting that preferential subsurface saturation may have contributed to the pockets of low resistivity seen in the two-dimensional seep tomogram. Also, the water table in the 4-m observation piezometer was 0.8 m below the surface on April 21, 2012 ($t_0$ in Figure 5), indicating possible saturation from the groundwater system below the fragipan despite the dry antecedent moisture conditions.

### Changes in Resistivity and Site Conditions During the Wet-Up Period

Time-lapse ERI revealed interesting contrasts in resistivity in the seep and non-seep area that became readily apparent with successive rainfall events ($t_1$ through $t_4$ in Figures 4 and 5). Following the first storm event, which deposited 40.1 mm of rainfall over the course of three days (April 21 to 23, 2012) ($t_1$ and $t_2$ in Figure 3a), sequential ERI surveys on April 23 and 25, 2012 showed that resistivity in the upper 0.6 m of soil decreased by 10 to 25% in the non-seep area ($t_1$ and $t_2$ in Figure 4) and by 25 to 40% in the seep area ($t_1$ and $t_2$ in Figure 5). These resistivity declines likely resulted from infiltrating rainwater, which differentially increased the moisture content of the more hydraulically conductive soil horizons above the fragipan horizon at both sites. Indeed, surficial soil moisture (average TDR measurements for the upper 0.6 m) increased to a greater degree in the seep area following the first storm event, rising by 15% in the seep (27 to 42% from $t_0$ to $t_1$ in Figure 5) and by only 7% in the non-seep (18 to 25% from $t_0$ to $t_1$ in Figure 4). The 8% greater increase in soil moisture in the seep area led to a resistivity decline that was 15% lower in magnitude than what was observed in the non-seep area. Interestingly, the seep area also exhibited marked reductions in resistivity of 25 to 40% in several pockets between approximately 1 and 2 m depth in the inversions ($t_1$ and $t_2$ in Figure 5), with the region above 1 m showing little to no change in resistivity. This pattern was unique to the seep area, and appeared to indicate progressive saturation from below at these depths, which was evidenced by the fact that water tables in the 4-m observation piezometer rose from 0.8 to 0.2 m below ground level, and moisture contents 0.8 m below the surface increased to 50% immediately following the first rainfall event ($t_1$ in Figure 5).

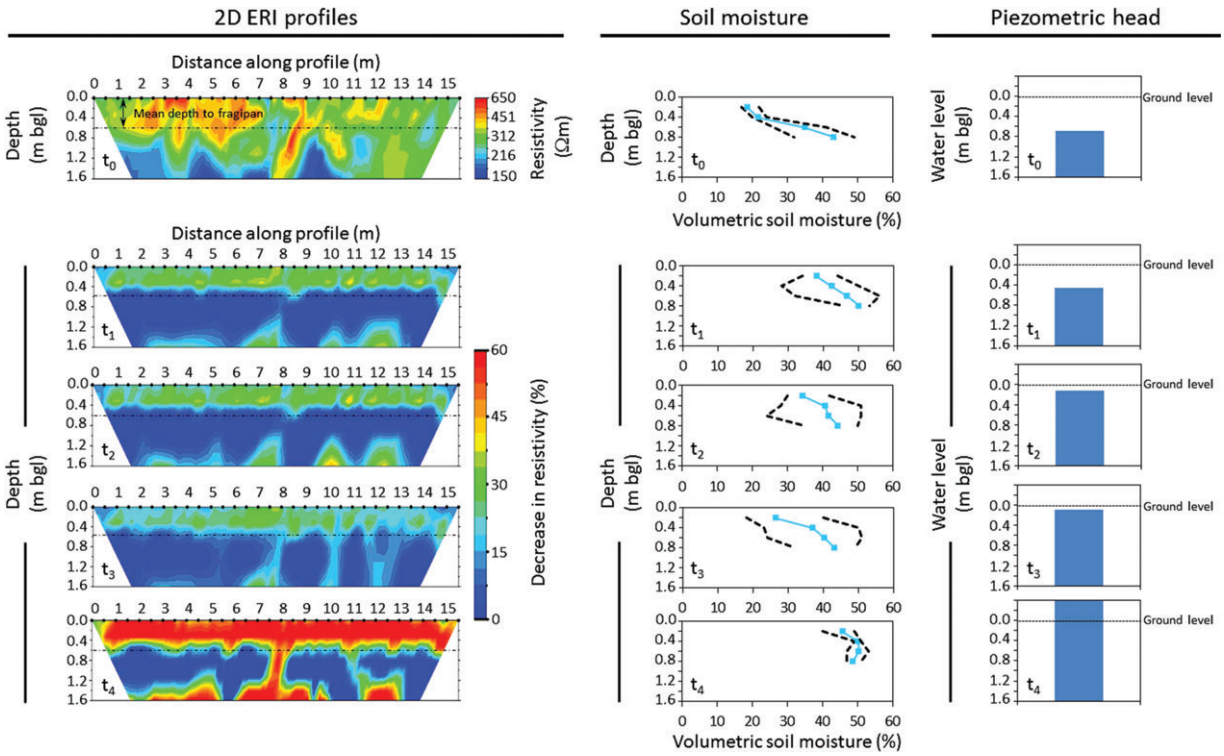


**Figure 5. Seep resistivity, soil moisture, and piezometric head (4-m piezometer) patterns for background conditions ($t_0$ = April 21, 2012) and four subsequent time steps over the wet-up period ($t_1$ = April 23, 2012; $t_2$ = April 25, 2012; $t_3$ = May 2, 2012; $t_4$ = May 21, 2012). Background resistivity data are given in Ωm, whereas resistivity difference inversions are shown as the percentage difference from background conditions. Volumetric soil moisture* is plotted as a function of depth, with minimum and maximum values shown as dashed black lines and the means shown as a solid blue line. Piezometric head is shown as water level depth (m) below ground level (bgl). *Volumetric soil moisture was measured with a Trime-FM TDR probe at three locations along the electrode transect, and mean, minimum, and maximum values were calculated across all three locations for each of the four depth intervals.**

The month of May 2012 featured several large storms that further amplified resistivity differences between seep and non-seep areas. For instance, the third ERI survey on May 2, 2012 immediately followed 6.1 mm of additional rainfall in the basin ($t_3$ in Figure 3a). While two-dimensional resistivity patterns in the non-seep area remained relatively unchanged from the two earlier surveys ($t_3$ in Figures 4 and 5), the seep area exhibited the early development of an interesting vertical anomaly between 7 and 8 m on the profile where resistivity declined by 10 to 20% ($t_3$ in Figure 5). Two more rainfall events on May 7 to 8, 2012 (30.7 mm) and May 14 to 15, 2012 (42.9 mm) brought the 1-month rainfall total to 141 mm and increased mean soil wetness at both sites to saturation ($\theta_{seep} = 48.5\%$; $\theta_{non\text{-}seep} = 45.8\%$) by May 21, 2012. On that date, ERI surveys ($t_4$ in Figure 5) showed that the vertical anomaly in the seep area had become even more pronounced, with resistivity reductions approaching 60% throughout the entire profile (decreasing from background levels of 150 to 250 Ωm through 50 to 150 Ωm on May 21, 2012). We observed resistivity reductions of a similar magnitude in the non-seep area (decreasing from background levels of 210 to 330 Ωm through 80 to 180 Ωm on May 21, 2012), but they were strictly confined to the area above the fragipan where a perched water table had developed ($t_4$ in Figure 4). Perhaps most notable was the apparent connection between the shallow fractured aquifer below the fragipan and the perched water system above as indicated by resistivity tomogram from the seep area, signifying a potentially dynamic interaction between these two systems that possibly was facilitated by a discontinuity in the fragipan horizon.

### Perspectives on Riparian Seep Hydrology Using Time-Lapse ERI and Hydrometric Data

The saturated conditions on May 21, 2012 afforded a holistic perspective of the hydrology and water quality of seep and non-seep areas of the riparian zone. In the seep area, the vertically oriented anomaly of reduced resistivity at the midpoint of the ERI transect (Figure 6a) aligned with areas where the piezometric surface, inferred with 0.2-m piezometers, was above ground level (Figure 6b), and where hydraulic head differentials were largely positive (≥2 cm) (Figure 6c). These collective trends pointed to groundwater upwelling from the shallow fractured aquifer where it then mixed with perched groundwater and eventually discharged to the surface. Indeed, piezometric head in the 4-m piezometer was 0.4 m above ground level in the seep area ($t_4$ in Figure 4), suggesting the potential for groundwater discharge. As indicated earlier, the groundwater system below the fragipan is likely artesian (Figure 3e), and therefore discontinuities in the

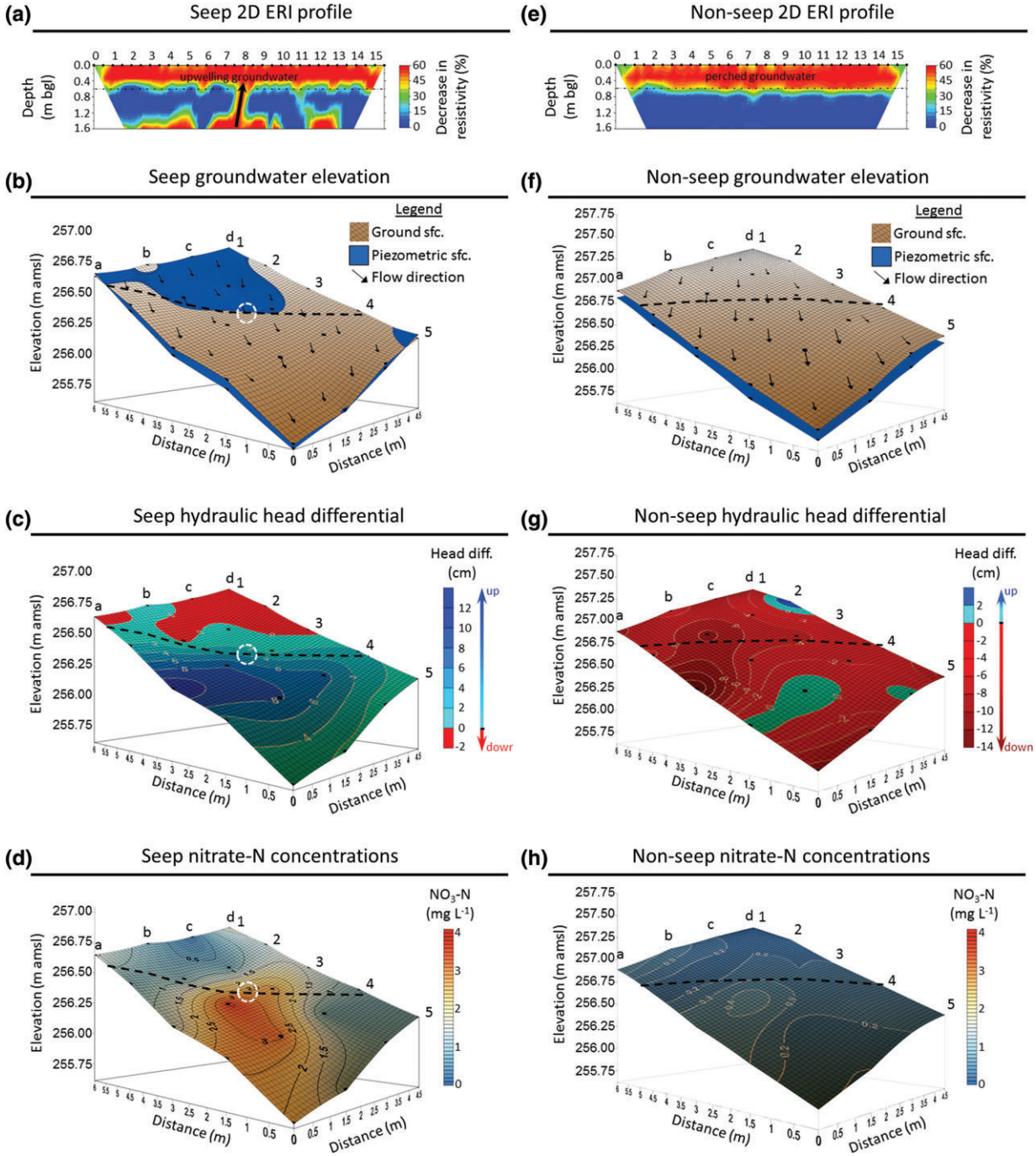


**Figure 6. Seep and non-seep hydrological and water quality conditions on May 21, 2012 ($t_4$). Four graphics are shown for each study location (seep = a through d; non-seep = e through h), including the two-dimensional resistivity difference inversion and a series of three-dimensional land-surface representations with contours of groundwater elevations (inferred from the 0.2-m piezometers), hydraulic head differentials (cm), and shallow groundwater nitrate-N concentrations (mg/L) plotted as map overlays. The dashed black line on the land-surface images represents the location of the ERI transects in seep and non-seep areas. For the seep area land-surface images, the dashed white circle indicates the approximate location of the vertically oriented resistivity anomaly shown in the resistivity difference inversion.**

fragipan may allow upward migration of deeper groundwater to the surface. Because the deeper groundwater system possesses elevated nitrate-N levels from upslope agriculture (Pionke and Urban 1985; Gburek and Folmar 1999), irregularities in fragipan architecture may provide a pathway for nitrate-N delivery to the seep (Figure 6d) and ultimately to the stream (Williams et al. 2014).

In stark contrast, ERI data from the non-seep area indicated that groundwater was perched above the fragipan, and had no apparent connection with the deeper groundwater system below (Figure 6e). The piezometric surface mapped with the 0.2-m piezometers was largely below ground level throughout the non-seep area (Figure 6f), and piezometric head in the 4-m piezometer

did not indicate the potential for groundwater discharge to the surface ($t_4$ in Figure 5) as was observed in the adjacent seep area. Moreover, lateral hydraulic gradients were directed downslope (Figure 6f), and hydraulic head differentials were strongly downward ($\leq -2$ cm; Figure 6g). Thus, rainfall from previous storm events likely was percolating through the profile, perching above the fragipan, and moving laterally downslope toward the stream. Lacking any obvious contributions from the nitrate-rich groundwater system below, nitrate-N concentrations in perched groundwater in the non-seep area remained largely below 0.4 mg/L (Figure 6h). The background ERI data and subsequent difference inversions during the wet-up period confirmed the homogenous nature of the fragipan horizon in the non-seep area, which effectively served to separate local and regional groundwater systems in this region of the riparian zone.

## Implications and Conclusions

Applying time-lapse ERI allowed us to delineate and describe hydrologic and pedogenic factors affecting groundwater flow and discharge in the riparian area of a small agricultural headwater basin in the Valley and Ridge region of Pennsylvania. At the non-seep location, 141 mm of rainfall from April to May 2012 led to a 28% increase in moisture content and a resultant 60% decline in resistivity in the 0.6-m area of soil above the fragipan, with the regional water table remaining well below the 1.6-m depth of ERI investigation. Thus, evidence from the non-seep area pointed to the development a perched water table that was hydraulically disconnected from the shallow fractured aquifer below. The upper 0.6 m of soil in the seep area responded similarly to the non-seep area, with rainfall inputs over the 1-month period producing resistivity reductions of 60% and attendant soil moisture increases of 22%. More importantly, however, we also mapped a vertically aligned region of the soil profile with resistivity declines of 60% that coincided with strong upward hydraulic gradients recorded in a grid of nested piezometers (0.2- and 0.6-m depth). This pattern suggested a hydraulic connection between the seep and the shallow groundwater system below the fragipan that enabled groundwater and associated nitrate-N to discharge through the fragipan to the land surface. Time-lapse ERI results from the seep area of FD-36 are strikingly consistent with recent geoelectrical studies in the UK, where ERI surveys of large wetland complexes underlain by peat have mapped heterogeneities in peat architecture, including the presence of gravels, that provide preferential pathways for upwelling groundwater (Chambers et al. 2014; Uhlemann et al. 2016).

Findings from our study suggest a possible role of fragipan architecture on the location and activation of riparian seeps in the Valley and Ridge province. Fragipan soils in headwater basins like FD-36 are notably heterogeneous (Grossman and Carlisle 1969), with several studies indicating anisotropy in saturated hydraulic conductivity (Parlange et al. 1989; Day et al. 1998), especially in the vertical direction (Dabney and Selim 1987), due to vertically oriented cracks and cleavage that are common to fragipan horizons. Individual cracks and cleavage features were likely less than the electrode spacing of 0.5 m, which precluded their precise delineation with ERI. Certainly, estimating a priori the scale of variability that would not be identified with ERI was difficult, as spatial resolution is an unknown function of many variables, including electrode geometry, measurement schedule, and the subsurface electrical conductivity distribution (Daily and Ramirez 1995). Even so, the vertically positioned resistivity anomaly in the seep area, which was unmapped in the non-seep area, showed that the 0.5-m electrode spacing used in our study was sufficient to detect the collective influence of cracks and cleavage structures in the fragipan and demonstrate their role as preferential groundwater flow pathways for confined aquifer discharge and nitrate-N efflux to riparian seeps.

Of course, the interpretation of ERI data should be made carefully in any situation, and our study is no exception. One drawback of our approach was the use of single electrode transects through seep and non-seep areas, which limited us to viewing three-dimensional processes as two-dimensional changes in resistivity over time. Future studies employing time-lapse ERI in the study of riparian seeps may consider an approach like that of Toran et al. (2015), where three-dimensional ERI surveys were used to identify zones of groundwater seepage in lakebeds. Nevertheless, comparing two-dimensional changes in geophysical response over time, an inherent strength of the time-lapse ERI method (Binley et al. 2010, 2015), still permitted meaningful interpretations of subsurface hydrological processes in seep and non-seep areas of the riparian zone. These interpretations were strengthened significantly by applying insight from supportive hydrologic datasets, including depth-varying soil moisture and routine groundwater monitoring at seep and non-seep sites, as well as continuous hydrologic data from nearby locations. Equally important was our ability to maintain the experimental setup, undisturbed, for the duration of the 1-month study period. In closing, our study demonstrates that time-lapse ERI methods offer valuable insight into the role of soil architecture on the hydrological functions of riparian seeps, and when paired with multiple lines of evidence from hydrometric and water quality monitoring, can shed additional light on groundwater and nutrient flow pathways to seeps in near-stream areas of headwater catchments.

## Acknowledgments

Mention of trade names or commercial products in this publication is solely for the purpose of providing specific information and does not imply recommendation or endorsement by the U.S. Department of Agriculture (USDA). USDA is an equal opportunity provider and employer. It prohibits discrimination in all its programs and activities on the basis of race, color, national origin, age, disability, and where applicable, sex, marital status,

familial status, parental status, religion, sexual orientation, genetic information, political beliefs, reprisal, or because all or part of an individual's income is derived from any public assistance program. (Not all prohibited bases apply to all programs.) Persons with disabilities who require alternative means for communication of program information (Braille, large print, audiotape, etc.) should contact USDA's TARGET Center at (202) 720-2600 (voice and TDD). To file a complaint of discrimination, write to USDA, Director, Office of Civil Rights, 1400 Independence Avenue, S.W., Washington, D.C. 20250-9410, or call (800) 795-3272 (voice) or (202) 720-6382 (TDD). USDA is an equal opportunity provider and employer.

## References


Alexander, R.B., E.W. Boyer, R.A. Smith, G.E. Schwarz, and R.B. Moore. 2007. The role of headwater streams in downstream water quality. *Journal of the American Water Resources Association* 43, no. 1: 41–59. DOI:10.1111/j.1752-1688.2007.00005.x.

Angier, J.T., and G.W. McCarty. 2008. Variations in baseflow nitrate flux in a first order stream and riparian zone. *Journal of the American Water Resources Association* 44, no. 2: 367–380. DOI:10.1111/j.1752-1688.2007.00153.x.

Binley, A., G. Cassiani, and R. Deiana. 2010. Hydrogeophysics: Opportunities and challenges. *Bollettino di Geofisica Teorica ed Applicata* 51, no. 4: 267–284.

Binley, A., S.S. Hubbard, J.A. Huisman, A. Revil, D.A. Robinson, K. Singha, and L.D. Slater. 2015. The emergence of hydrogeophysics for improved understanding of subsurface processes over multiple scales. *Water Resources Research* 51: 3837–3866. DOI:10.1002/2015WR017016.

Brinson, M.M. 1993. A hydrogeomorphic classification for wetlands. Wetlands Research Program Technical Report WRP-DE-4, Vicksburg, Mississippi: U.S. Army Corps of Engineers.

Bryant, R.B., T.L. Veith, G.W. Feyereisen, A.R. Buda, C.D. Church, G.J. Folmar, J.P. Schmidt, C.J. Dell, and P.J.A. Kleinman. 2011. US Department of Agriculture Agricultural Research Service Mahantango Creek Watershed, Pennsylvania, United States: Physiography and history. *Water Resources Research* 47: W08701. DOI:10.1029/2010WR010056.

Buda, A.R., T.L. Veith, G.J. Folmar, G.W. Feyereisen, R.B. Bryant, C.D. Church, J.P. Schmidt, C.J. Dell, and P.J.A. Kleinman. 2011. U.S. Department of Agriculture Agricultural Research Service Mahantango Creek Watershed, Pennsylvania, United States: Long-term precipitation database. *Water Resources Research* 47: W08702. DOI:10.1029/2010WR010058.

Burns, D.A., P.S. Murdoch, G.B. Lawrence, and R.L. Michel. 1998. Effect of groundwater springs on $NO_3^-$ concentrations during summer in Catskill Mountain streams. *Water Resources Research* 34, no. 8: 1987–1996. DOI:10.1029/98WR01282.

Cardenas, M.B., and M.S. Markowski. 2011. Geoelectrical imaging of hyporheic exchange and mixing of river water and groundwater in a large regulated river. *Environmental Science and Technology* 45, no. 4: 1407–1411. DOI:10.1021/es103438a.

Cassiani, G., A. Godio, S. Stocco, A. Villa, R. Deiana, P. Frattini, and M. Rossi. 2009. Monitoring the hydrologic behavior of a mountain slope via time-lapse electrical resistivity tomography. *Near Surface Geophysics* 7, no. 5–6: 475–486. DOI:10.3997/1873-0604.2009013.

Chambers, J.E., P.B. Wilkinson, S. Uhlemann, J.P.R. Sorenson, C. Roberts, A.J. Newell, W.O.C. Ward, A. Binley, P.J. Williams, D.C. Gooddy, G. Old, and L. Bai. 2014. Derivation of lowland riparian wetland deposit architecture using geophysical image analysis and interface detection. *Water Resources Research* 50: 5886–5905. DOI:10.1002/2014WR015643.

Ciolkosz, E.J., G.W. Peterson, R.L. Cunningham, and R.P. Matelski. 1979. Soils derived from colluvium in the Ridge and Valley area of Pennsylvania. *Soil Science* 128, no. 3: 153–162.

Ciolkosz, E.J., B.J. Carter, M.T. Hoover, R.C. Cronce, W.J. Waltman, and R.R. Dobos. 1990. Genesis of soils and landscapes in the Ridge and Valley province of central Pennsylvania. *Geomorphology* 3: 245–261. DOI:10.1016/0169-555X(90)90006-C.

Dabney, S.M., and H.M. Selim. 1987. Anisotropy of a fragipan horizon: Vertical vs. horizontal hydraulic conductivity. *Soil Science Society of America Journal* 51: 3–6. DOI:10.2136/sssaj1987.03615995005100010001x.

Daily, W., and A. Ramirez. 1995. Electrical resistance tomography during in-situ trichloroethylene remediation at the Savannah River site. *Journal of Applied Geophysics* 33, no. 4: 239–249. DOI:10.1016/0926-9851(95)90044-6.

Daily, W.D., A.L. Ramirez, D.J. LaBrecque, and J. Nitao. 1992. Electrical resistivity tomography of vadose water movement. *Water Resources Research* 28: 1429–1442. DOI:10.1029/91WR03087.

Day, R.L., M.A. Calmon, J.M. Stiteler, J.D. Jabro, and R.L. Cunningham. 1998. Water balance and flow patterns in a fragipan using in situ soil block. *Soil Science* 163, no. 7: 517–528.

Doestch, J., N. Linde, T. Vogt, A. Binley, and A.G. Green. 2012. Imaging and quantifying salt-tracer transport in a riparian groundwater system by means of 3D ERT monitoring. *Geophysics* 77: B207–B218. DOI:10.1190/geo2012-0046.1.

Gburek, W.J., and G.J. Folmar. 1999. Flow and chemical contributions to streamflow in an upland watershed: A baseflow survey. *Journal of Hydrology* 217: 1–18. DOI:10.1016/S0022-1694(98)00282-0.

Gburek, W.J., and J.B. Urban. 1990. The shallow weathered fracture layer in the near-stream zone. *Groundwater* 28, no. 6: 875–883. DOI:10.1111/j.1745-6584.1990.tb01723.x.

Gburek, W.J., G.J. Folmar, and J.B. Urban. 1999. Field data and ground water modeling in a layered fractured aquifer. *Groundwater* 37, no. 2: 175–184. DOI:10.1111/j.1745-6584.1999.tb00972.x.

Gburek, W.J., B.A. Needelman, and M.S. Srinivasan. 2006. Fragipan controls on runoff generation: Hydropedological implications at landscape and watershed scales. *Geoderma* 131: 330–344. DOI:10.1016/j.geoderma.2005.03.021.

Gentry, W.M., and T.J. Burbey. 2004. Characterization of ground water flow from spring discharge in a crystalline rock environment. *Journal of the American Water Resources Association* 40, no. 5: 1205–1217. DOI:10.1111/j.1752-1688.2004.tb01580.x.

Geyer, A.R., and J.P. Wilshusen. 1982. Engineering characteristics of the rocks of Pennsylvania. Environmental Geology Report 1. Pennsylvania Department of Environmental Resources and Bureau of Topographic and Geologic Survey. Harrisburg, Pennsylvania: Pennsylvania Geologic Survey. 294 p.

Gregory, S.V., F.J. Swanson, W.A. McKee, and K.W. Cummins. 1991. An ecosystem perspective of riparian zones. *BioScience* 41, no. 8: 540–551. DOI:10.2307/1311607.

Grossman, R.B., and F.J. Carlisle. 1969. Fragipan soils of the Eastern United States. *Advances in Agronomy* 21: 237–279. DOI:10.1016/S0065-2113(08)60099-1.

Gurdak, J.J., and S.L. Qi. 2012. Vulnerability of recently recharged groundwater in principle aquifers of the

United States to nitrate contamination. *Environmental Science and Technology* 46, no. 11: 6004–6012. DOI:10.1021/es300688b.

Hayley, K., L.R. Bentley, M. Gharibi, and M. Nightingale. 2007. Low temperature dependence of electrical resistivity: Implications for near surface geophysical monitoring. *Geophysical Research Letters* 34: L18402. DOI:10.1029/2007GL031124.

Heathwaite, L., A.N. Sharpley, and W.J. Gburek. 2000. A conceptual approach for integrating phosphorus and nitrogen management at watershed scales. *Journal of Environmental Quality* 29, no. 1: 158–166. DOI:10.2134/jeq2000.00472425002900010020x.

Hill, A.R. 1990. Groundwater flow paths in relation to nitrogen chemistry in the near-stream zone. *Hydrobiologia* 206, no. 1: 39–52. DOI:10.1007/bf00018968.

Kaur, A.J., D.S. Ross, J.B. Shanley, and A.R. Yatzor. 2016. Enriched groundwater seeps in two Vermont headwater catchments are hotspots of nitrate turnover. *Wetlands* 36, no. 2: 237–249. DOI:10.1007/s13157-016-0733-z.

Keller, G.V., and F.C. Frischknecht. 1966. Electrical methods of geophysical prospecting. *International Series of Monographs of Electromagnetic Waves* 10: 1–33.

Leslie, I.N., and R. Heinse. 2013. Characterizing soil-pipe networks with pseudo-three-dimensional resistivity tomography on forested hillslopes with restrictive horizons. *Vadose Zone Journal* 12: 1–10. DOI:10.2136/vzj2012.0200.

Lindeburg, K.S. 2011. Silty mantles and fragipans in Pennsylvania soils. M.S. thesis in Soil Science, The Pennsylvania State University, State College, Pennsylvania, 257 pp.

Loke, M.H. 2015. Electrical imaging surveys for environmental and engineering studies: a practical guide to 2-D and 3-D surveys. Unpublished lecture notes, Available through Geotomo Software. http://www.geotomosoft.com (accessed June 13, 2016).

Lu, H., R.B. Bryant, A.R. Buda, A.S. Collick, G.J. Folmar, and P.J.A. Kleinman. 2015. Long-term trends in climate and hydrology in an agricultural, headwater watershed of central Pennsylvania, USA. *Journal of Hydrology: Regional Studies* 4: 713–731. DOI:10.1016/j.ejrh.2015.10.004.

Martínez-Santos, M., E. Ruíz-Romera, M. Martínez-López, and I. Antigüedad. 2012. Influence of upwelling on the shallow water chemistry in a small wetland riparian zone (Basque Country). *Applied Geochemistry* 27: 854–865. DOI:10.1016/j.apgeochem.2012.01.007.

Morley, T.R., A.S. Reeve, and A.J.K. Calhoun. 2011. The role of headwater wetlands in altering streamflow and chemistry in Maine, USA. *Journal of the American Water Resources Association* 47, no. 2: 337–349. DOI:10.1111/j.1752-1688.2010.00519.x.

Nadeau, T.-L., and M.C. Rains. 2007. Hydrological connectivity between headwater streams and downstream waters: How science can inform policy. *Journal of the American Water Resources Association* 43, no. 1: 118–133. DOI:10.1111/j.1752-1688.2007.00010.x.

O'Driscoll, M.A., and D.R. DeWalle. 2010. Seeps regulate stream nitrate concentration in forested Appalachian catchments. *Journal of Environmental Quality* 39, no. 1: 420–431. DOI:10.2134/jeq2009.0083.

Parlange, M.B., T.S. Steenhuis, D.J. Timlin, F. Stagnitti, and R.B. Bryant. 1989. Subsurface flow above a fragipan horizon. *Soil Science* 148, no. 2: 77–86.

Parsekian, A.D., K. Singha, B.J. Minsley, W.S. Holbrook, and L. Slater. 2014. Multiscale geophysical imaging of the critical zone. *Reviews of Geophysics* 53, no. 1: 1–26. DOI:10.1002/2014RG000465.

Pionke, H.B., and J.B. Urban. 1985. Effect of agriculture land use on ground-water quality in a small Pennsylvania watershed. *Groundwater* 23: 68–80. DOI:10.1111/j.1745-6584.1985.tb02781.x.

Samouëlian, A., I. Cousin, A. Tabbagh, A. Bruand, and G. Richard. 2005. Electrical resistivity survey in soil science: a review. *Soil and Tillage Research* 83: 173–193. DOI:10.1016/j.still.2004.10.004.

Saxton, K.E., and W.J. Rawls. 2006. Soil water characteristic estimates by texture and organic matter for hydrologic solutions. *Soil Science Society of America Journal* 70, no. 5: 1569–1578. DOI:10.2136/sssaj2005.0117.

Singha, K., F.D. Day-Lewis, T. Johnson, and L.D. Slater. 2015. Advances in interpretation of subsurface processes with time-lapse electrical imaging. *Hydrological Processes* 29: 1549–1576. DOI:10.1002/hyp.10280.

Soil Survey Staff. 2014. Kellogg Soil Survey Laboratory Methods Manual. Soil Survey Investigations Report 42, Version 5.0. R. Burt and Soil Survey Staff, eds. Washington, D.C: U.S. Department of Agriculture, Natural Resources Conservation Service.

Stein, E.D., M. Mattson, A.E. Fetscher, and K.J. Halama. 2004. Influence of geologic setting on slope wetland hydrodynamics. *Wetlands* 24, no. 2: 244–260. DOI:10.1672/0277-5212(2004)024[0244:iogsos]2.0.co;2.

Toran, L., J. Nyquist, D. Rosenberry, M. Gagliano, N. Mitchell, and J. Mikochik. 2015. Geophysical and hydrologic studies of lake seepage variability. *Groundwater* 53, no. 6: 841–850. DOI:10.1111/gwat.12309.

Uhlemann, S.S., J.P.R. Sorenson, A.R. House, P.B. Wilkinson, C. Roberts, D.C. Gooddy, A.M. Binley, and J.E. Chambers. 2016. Integrated time-lapse geoelectrical imaging of wetland hydrological processes. *Water Resources Research* 52, no. 3: 1607–1625. DOI:10.1002/2015WR017932.

Vidon, P.G.F., and A.R. Hill. 2004a. Landscape controls on the hydrology of stream riparian zones. *Journal of Hydrology* 292, no. 1–4: 210–228. DOI:10.1016/j.jhydrol.2004.01.005.

Vidon, P.G.F., and A.R. Hill. 2004b. Landscape controls on nitrate removal in stream riparian zones. *Water Resources Research* 40: 3. DOI:10.1029/2003WR002473.

Ward, A.S., M.N. Gooseff, and K. Singha. 2010. Imaging hyporheic zone solute transport using electrical resistivity. *Hydrological Processes* 24, no. 7: 948–953. DOI:10.1002/hyp.7672.

West, A.J., S.E. Findlay, D.A. Burns, K.C. Weathers, and C.M. Lovett. 2001. Catchment-scale variation in the nitrate concentration of groundwater seeps in the Catskill Mountains, New York, USA. *Water, Air, and Soil Pollution* 132: 389–400. DOI:10.1023/a:1013268004513.

Williams, M.R., A.R. Buda, H.A. Elliott, J. Hamlett, E.W. Boyer, and J.P. Schmidt. 2014. Groundwater flow path dynamics and nitrogen transport potential in the riparian zone of an agricultural headwater catchment. *Journal of Hydrology* 511: 870–879. DOI:10.1016/j.jhydrol.2014.02.033.

Williams, M.R., A.R. Buda, H.A. Elliott, A.S. Collick, C. Dell, and P.J.A. Kleinman. 2015. Linking nitrogen management, seep chemistry, and stream water quality in two agricultural headwater watersheds. *Journal of Environmental Quality* 44, no. 3: 910–920. DOI:10.2134/jeq2014.10.0412.

Winter, T.C. 1988. A conceptual framework for assessing cumulative impacts on the hydrology of nontidal wetlands. *Environmental Management* 12, no. 5: 605–620. DOI:10.1007/bf01867539.

Winter, T.C., J.W. Harvey, O.L. Franke, and W.M. Alley. 1998. Ground water and surface water: a single resource. U.S. Geological Survey Circular 1139, 79 pp.

Wyrick G.G., and J.W. Borchers. 1981. Hydrological effects of stress-relief fracturing in an Appalachian valley. U.S. Geological Survey Water-Supply Paper 2177, 51 pp.